Applied Surface Science Advances 31 (2026) 100925

Contents lists available at ScienceDirect

Applied Surface Science Advances

journal homepage: www.sciencedirect.com/journal/applied-surface-science-advances

Effect of $NaBH_4$ loading and reduction temperature on defect-driven CO_2 photoreduction over TiO_2

Rudolf Ricka [a,b], Agnieszka Wanag [c], Ewelina Kusiak-Nejman [c], Martin Reli [a], Miroslava Filip Edelmannová [a], Marcin Łapinski [d], Grzegorz Słowik [e], Antoni W. Morawski [c], Kamila Kočí [a,f,*]

[a] Institute of Environmental Technology, CEET, VSB-Technical University of Ostrava, 17. listopadu 2172/15, 708 00 Ostrava-Poruba, Czech Republic
[b] Faculty of Materials Science and Technology, VSB-Technical University of Ostrava, 17. listopadu 2172/15, 708 00 Ostrava-Poruba, Czech Republic
[c] Department of Inorganic Chemical Technology and Environment Engineering, Faculty of Chemical Technology and Engineering, West Pomeranian University of Technology in Szczecin, ul. Pułaskiego 10, 70-322 Szczecin, Poland
[d] Institute of Nanotechnology and Materials Engineering, Faculty of Applied Physics and Mathematics, Gdańsk University of Technology, Narutowicza 11/12, 80-233 Gdańsk, Poland
[e] Department of Chemical Technology, Faculty of Chemistry, Maria Curie-Skłodowska University, 3. Maria-Curie-Skłodowska Sq., 20-031 Lublin, Poland
[f] Department of Physics and Materials Engineering, Faculty of Technology, Tomas Bata University in Zlín, Vavrečkova 275, Czech Republic

ARTICLE INFO

Keywords:
TiO_2
Defect engineering
Ti^{3+} sites
Oxygen vacancies
CO_2 reduction
photocatalysis

ABSTRACT

This study investigates the role of defect engineering in enhancing TiO_2-based photocatalysts for CO_2 photoreduction through a systematically controlled synthesis. In contrast to previous reports focused on Ti^{3+} doping of commercial TiO_2, here we combine sol–gel synthesis with post-synthetic chemical reduction using sodium borohydride ($NaBH_4$) to obtain TiO_2 materials with tunable concentrations of surface defects, specifically oxygen vacancies and Ti^{3+} sites. By varying both the reduction temperature and $NaBH_4$ dosage, we introduce a new level of control over defect formation. The materials were characterized by X-ray diffraction (XRD), Raman spectroscopy, transmission electron microscopy (TEM), X-ray photoelectron spectroscopy (XPS), nitrogen physisorption, and photoelectrochemical measurements. Photocatalytic performance was assessed via CO_2 photoreduction under UV–vis irradiation. The sample reduced at 350 °C with 1.5 *g* $NaBH_4$ showed the highest activity and selectivity toward CH_4 and CO, clearly surpassing the performance of commercial TiO_2 (P25) and a sol–gel reference without chemical reduction (W-TiO_2_350 °C). The improved performance is attributed to a synergistic balance of Ti^{3+} sites, oxygen vacancies, and surface hydroxyls, which enhance charge separation and CO_2 activation. This work introduces new synthesis–structure–activity relationships and demonstrates the potential of defect-tuned TiO_2 materials for efficient and selective CO_2 valorization.

1. Introduction

On the one hand, carbon dioxide is a colourless gas used in the chemical and food industries [1–3]. On the other hand, it is one of the major greenhouse gases, contributing to global warming and climate change. As demonstrated by data published by NASA, the concentration of CO_2 in the atmosphere measured in July 2024 was 427 ppm, the highest level in the last 60 years [4]. Moreover, given the ongoing population growth and the development of industrialization, it appears that the upward trend will not change in the future and the concentration of CO_2 molecules in the atmosphere will continue to rise [5,6]. Based on these insights, it is essential to develop novel CO_2 utilization strategies, and photocatalytic CO_2 reduction could potentially be one of them.

Photocatalytic CO_2 reduction is a promising strategy in the fight against the ongoing energy crisis, global warming, and climate change. The key advantage of this technology lies in the direct conversion of CO_2 molecules into high-density chemical energy through photochemical reactions induced by the interaction between photocatalytically active materials and light energy [7,8]. However, despite its great potential, the path to practical application is still far. The main issue in this field is related to the low level of CO_2 conversion. Indeed, the CO_2 molecule is

* Corresponding author.
E-mail address: kamila.koci@vsb.cz (K. Kočí).

https://doi.org/10.1016/j.apsadv.2025.100925
Received 21 July 2025; Received in revised form 18 November 2025; Accepted 23 December 2025
Available online 6 January 2026

very stable, and disrupting the $C = O$ bonds within this molecule is very challenging [9–11]. Based on these insights, it is essential to find ways to increase the currently low CO_2 conversion level, which could lead to improved efficiency of the CO_2 photoreduction process. Fortunately, one of the most effective ways to improve the level of CO_2 conversion is through the design and synthesis of efficient photocatalytically active materials, such as the defect-based TiO_2 photocatalysts, which are the primary photocatalysts studied in this research [12].

TiO_2 is one of the most studied materials in the field of photocatalysis. While it offers several advantages, including low cost and excellent thermal and chemical stability, its wide band gap (3.2 eV) and high charge carrier recombination rate significantly limit its photocatalytic applications [13–16]. To overcome these limitations, the physico-chemical properties of this material must be modified to enhance its potential for broader utilization in photocatalysis. Fortunately, defect engineering represents one of the most promising approaches for modifying photocatalysts. The successful introduction of surface defects into TiO_2, such as oxygen vacancies and Ti^{3+} states, enhances its light absorption efficiency, facilitates charge carrier separation, and consequently improves its performance in CO_2 photoreduction [7,17–20]. These, defective states can be introduced using various reduction methods, including direct hydrogenation or chemical reduction, which permit the controlled formation of these defective states [21].

In recent years, defect-engineered and black TiO_2 photocatalysts have attracted significant attention for photocatalytic CO_2 conversion due to their ability to extend light absorption into the visible region and promote efficient charge separation. For example, hydrogenated or chemically reduced TiO_2 with oxygen vacancies and Ti^{3+} species has exhibited enhanced CO_2 to CO and CH_4 yields compared to pristine TiO_2 [22]. Similarly, defect-rich TiO_2 prepared under controlled reduction conditions showed that the concentration of oxygen vacancies and Ti^{3+}/Ti^{4+} ratio strongly influences the photocatalytic efficiency [23]. More recently, Katai et al. [24] demonstrated that optimizing both defect density and crystal orientation can synergistically enhance CO_2 adsorption and activation. Other works have also reported that black TiO_2 with tailored the Ti^{3+} and vacancy concentrations improves charge separation and visible-light absorption, resulting in higher CO_2 conversion rates [25].

Besides defect formation, successful metal doping (for example Au, Pd, Pt) and the formation of heterojunctions represent other effective approaches to improve the photocatalytic efficiency of defective TiO_2 for CO_2 photoreduction. These strategies not only promote the separation and transfer of photogenerated charge carriers, but also form new active sites and favourable band alignments, resulting in synergistic effects and enhanced CO_2 photoreduction performance [26–31].

The growing interest in defect-based photocatalysts for CO_2 photoreduction is also supported by several recently published studies that have dealt not only with defective TiO_2 photocatalysts, but also other defect-based systems, such as defective ZnAl-LDH [32], g-C_3N_4/CeO_2 [33], or NH_2-UiO-66-MOF materials [34]. Despite these advances, the relationship between the type and concentration of surface defects, the preparation parameters, and the resulting photocatalytic performance is still not fully understood. Future research should focus, in particular, on a thorough investigation of defect dynamics and their influence on CO_2 photoreduction, as well as on the design and synthesis of new multi-defective photocatalysts to explore potential synergistic effects among different types of defects and their impact on CO_2 photoreduction performance [35].

In this study, we synthesized defect-based TiO_2 photocatalysts by combining the sol-gel technique with $NaBH_4$ reduction. The prepared TiO_2-based samples underwent extensive characterization using various analytical techniques to obtain detailed insights into their physico-chemical properties. Subsequently, the photocatalytic performance of the synthesized samples was evaluated for CO_2 reduction and compared to the activity of the commercial TiO_2 sample P25, which serves as a benchmark in the field of photocatalysis. Moreover, the photocatalytic performance of the most active Black-TiO_2-based (B-TiO_2) photocatalyst, B-TiO_2_350 °C_1.5, was compared with the additionally prepared reference sample White-TiO_2_350 °C_1.5 (W-TiO_2), which lacks a rich defect structure. This work establishes a systematic strategy for defect tuning in TiO_2 and focuses on evaluating the relationship between the photocatalyst structure and CO_2 photoreduction activity as a function of defect concentration and photocatalytic performance. It provides a deeper understanding of the coexistence and combined influence of Ti^{3+} sites and oxygen vacancies on the CO_2 photoreduction process. Furthermore, this work underscores the often-overlooked role of surface hydroxyl ($O_{O—H}$) groups and their interplay with defects, which significantly influence charge transfer, reactant adsorption, and the final efficiency of CO_2 photoreduction.

2. Experimental section

2.1. Materials

Titanium(IV) isopropoxide (TTIP) (≥97 %, Sigma-Aldrich Co., Saint Louis, MO, USA) was used as a TiO_2 precursor. Sodium borohydride ($NaBH_4$), purchased from Merck KGaA (Germany), was used as the reducing agent. Ethanol (C_2H_5OH), used for washing the photocatalyst samples, was purchased from P. P. H. "STANLAB" Sp. z.o.o., (Poland).

2.2. Synthesis of B-TiO_2_350 °C_0.75, B-TiO_2_350 °C_1.5, and B-TiO_2_350 °C_2.0 samples

B-TiO_2 photocatalysts with varying loading of the reducing agent $NaBH_4$ were prepared using the sol-gel technique followed by the $NaBH_4$ chemical reduction. The three synthesized photocatalyst samples, labelled B-TiO_2_350 °C_0.75, B-TiO_2_350 °C_1.5, and B-TiO_2_350 °C_2.0, were prepared using 0.75 g, 1.5 g, and 2.0 g of $NaBH_4$ as the reducing agent, corresponding to $NaBH_4$/Ti molar ratios of (calculated from the Ti content in the TTIP precursor) 0.3: 1, 0.6: 1, and 0.8: 1. In the first step, 20 ml of TTIP and 5 ml of ethanol were mixed. Subsequently, 50 ml of ultrapure water was added dropwise into the flasks containing the mixtures prepared in the previous step. The resulting mixtures were then stirred for 24 h and aged for another 24 h. The obtained gel was then dried overnight at 90 °C in a drier. In the next step, 2 g of the obtained TiO_2 was ground with varying amounts of $NaBH_4$ (0.75 g, 1.5 g, and 2.0 g) using an agate mortar and pestle. The mixtures were ground for 30 min. Afterwards, the mixtures were transferred to a tubular furnace, where they were heated up to 350 °C (temperature rate = 10 °C/min) and calcined at 350 °C under argon atmosphere (flow rate of Ar = 5 ml/min) for 1 hour. After calcination, the reduced Ti-based samples were cooled to room temperature and washed with ethanol and deionized water. Finally, the samples were dried at 70 °C in a drying furnace.

2.3. Synthesis of B-TiO_2_350 °C_1.5, B-TiO_2_500 °C_1.5, and B-TiO_2_650 °C_1.5 samples

The synthesis of B-TiO_2_350 °C_1.5, B-TiO_2_500 °C_1.5, and B-TiO_2_650 °C_1.5 photocatalysts follows the preparation procedure described in the previous Section 2.2. The only differences were the utilize of a 1.5 g $NaBH_4$ dosage, corresponding to the $NaBH_4$/Ti molar ratio of 0.6: 1, and the variation in temperature conditions during the $NaBH_4$ reduction of Ti-based sols. Specifically, the obtained sols were heated up to 350 °C, 500 °C, and 650 °C (temperature rate = 10 °C/min) and calcined at these temperatures under an argon atmosphere (Argon flow rate = 5 ml/min) in a tubular furnace for 1 hour.

2.4. Preparation of the reference W-TiO_2_350 °c sample

The individual steps for the preparation of the W-TiO_2_350 °C photocatalyst followed the synthesis procedure described in Section 2.2.

However, in this case, the obtained sol after aging was not ground with the $NaBH_4$ reducing agent, but was directly transferred to a tubular furnace, where it was heated to 350 °C, and calcined at this temperature for 1 hour in a glass crucible. Finally, it was cooled to room temperature and washed with ethanol and deionized water.

The list and images of the investigated TiO_2-based photocatalyst samples are shown in Table 1 and Figure S1.

2.5. Photocatalytic CO_2 reduction experiments

Photocatalytic testing of the investigated photocatalysts for CO_2 reduction was performed in a batch-stirred photoreactor (Figure S2). A detailed description of the performed CO_2 photoreduction experiments is provided in the Supplementary Materials.

2.6. Characterization of the prepared tio$_2$-based photocatalyst samples

The prepared TiO_2-based photocatalysts were characterized using advanced analytical methods, such as X-ray diffraction (XRD), Raman spectroscopy, transmission electron microscopy (TEM), X-ray photoelectron spectroscopy (XPS), N_2-physisorption, and photoelectric measurements (photocurrent). A detailed description of the performed characterization methods is given in the Supplementary Materials.

3. Results and discussion

3.1. Photocatalytic performance of the investigated photocatalysts

To evaluate the effectiveness of the prepared defect-rich TiO_2-based photocatalysts, photocatalytic testing over the investigated samples was performed. The data obtained from these experiments were further analyzed and correlated with results from characteristic techniques, revealing the physico-chemical properties of the samples. This analysis aims to clarify the influence of the individual parameters of the investigated photocatalysts on CO_2 photoreduction.

Photocatalytic CO_2 reduction experiments were conducted in a batch-stirred photoreactor (Figure S2). Carbon monoxide and methane, as the primary products of CO_2 photoreduction (Eq. (1) and 2), and hydrogen, as the main product of the competitive water splitting reaction (Eq. (3)), were detected [36,37].

$$CO_2 + 2H^+ + 2e^- \rightarrow CO + H_2O \quad (1)$$

$$CO_2 + 8H^+ + 8e^- \rightarrow CH_4 + 2H_2O \quad (2)$$

$$2H^+ + 2e^- \rightarrow H_2 \quad (3)$$

In this study, as shown in Fig. 1, the efficiency of the photocatalyst samples was evaluated as a function of two variables: the modulation in the amount of the used reducing agent ($NaBH_4$) and the variation in the reduction temperature during the $NaBH_4$ chemical reduction.

The results, depicted in the plots in Fig. 1a – b and Figure S3a – f, reveal the presence of two distinct trends. First, the photocatalytic activity of the investigated TiO_2-based samples increased with the increasing amount of $NaBH_4$ reducing agent used. This trend corresponds to the significant rise in the yields of detected products when using 1.5 g of $NaBH_4$ (B-TiO_2_350 °C_1.5) compared to 0.75 g (B-TiO_2_350 °C_0.75), which are noticeably lower. However, the experimental data also indicated that using 2.0 g of reducing agent during the reduction process led to a marked decline in the yields of products, resulting in lower photocatalytic activity. Second, the yields of carbonaceous products in the presence of defect-rich TiO_2-based photocatalysts decreased dramatically as the temperature used during the $NaBH_4$ reduction gradually increased. This trend is clearly apparent in Fig. 1b, which illustrates a significant drop in CO and CH_4 yields at reduction temperatures of 500 °C (B-TiO_2_500 °C_1.5) and 650 °C (B-TiO_2_650 °C_1.5), compared to the B-TiO_2_350 °C_1.5 sample, reduced at the temperature of 350 °C.

Table 1
The list of the synthesized TiO_2-based photocatalyst samples.

Sample order	Sample name
1	B-TiO_2_350 °C_0.75
2	B-TiO_2_350 °C_1.5
3	B-TiO_2_350 °C_2.0
4	B-TiO_2_500 °C_1.5
5	B-TiO_2_650 °C_1.5
6	W-TiO_2_350 °C

The stability of the investigated photocatalyst samples was verified by conducting repeated measurements of each sample at least four times. Specifically, the same batch containing the tested photocatalyst sample with a 0.2 M aqueous solution of sodium hydroxide was used repeatedly, and the mixture was saturated with CO_2 each time. The results were reproducible, confirming the stability of the photocatalyst samples. The measurement errors remained within 5 %, as reflected by the error bars highlighted in Fig. 1a – b.

3.2. Characterization of the investigated photocatalysts

As widely recognized, the photocatalytic efficiency of photocatalysts is closely linked to their physico-chemical properties. Based on this claim, it is essential to identify and clarify the potential influence of individual photocatalyst parameters on the photocatalytic activity of each sample, as summarized in the previous section. To achieve this, the tested nanomaterials underwent complex characterization using various analytical techniques.

As shown in Fig. 2a – c, XRD analysis confirms that the brookite phase predominates in all investigated samples, except the B-TiO_2_650 °C_1.5 sample. This observation aligns with the presence of the red-marked circles, which indicate XRD peaks corresponding to the brookite phase (PDF-2 card No 00–029–1360, Fig. 2a – c). In contrast, only the B-TiO_2_650 °C_1.5 sample exhibits a mixed-phase structure consisting of TiO (PDF-2 card No 00-009-0240, Fig. 2b), Ti_3O_5 (PDF-2 card No 01–082–117, Fig. 2b), and Hongquiit phase (PDF-2 card No 01–073–9518, Fig. 2b). Additionally, XRD analysis revealed the formation of a mixed phase in the samples B-TiO_2_350 °C_0.75 and the reference sample W-TiO_2_350 °C, both containing brookite and anatase phases (PDF-2 card No 01–075–2544, Fig. 2a and c).

Upon closer examination of Fig. 2a, it is evident that increasing the amount of $NaBH_4$ (from 0.75 g to 2.0 g) induces not only a transition of the phase structure from a mixed anatase-brookite phase to predominantly brookite, but also the emergence of an amorphous phase. This fact is primarily evidenced by the broadening of the detected XRD peaks. Moreover, this finding is also supported by TEM analysis of the most active sample B-TiO_2_350 °C_1.5, which demonstrates the coexistence of both crystalline TiO_2 and amorphous phases within the sample (Fig. 2d).

Furthermore, XRD analysis of the investigated samples B-TiO_2_350 °C_1.5, B-TiO_2_500 °C_1.5, and B-TiO_2_650 °C_1.5 reveals that increasing the temperature during the $NaBH_4$ chemical reduction not only leads to a slight increase in the crystallinity of the B-TiO_2-based samples, but also promotes the formation of multiphase crystalline structures. This observation is evident from the higher number of sharp XRD peaks in the patterns of the B-TiO_2 sample reduced at temperature 650 °C (B-TiO_2_650 °C_1.5 - green curve, Fig. 2b), compared to those reduced at 350 °C and 500 °C (B-TiO_2_350 °C_1.5 - blue curve; B-TiO_2_500 °C_1.5 - brown curve, Fig. 2b).

The defect-based sample B-TiO_2_350 °C_1.5 exhibited the highest photocatalytic activity among the prepared B-TiO_2-based samples. Considering this insight, it is crucial to compare its crystalline structure with that of the reference samples W-TiO_2_350 °C, which exhibited lower photocatalytic performance. As depicted in Fig. 2c, the crystal structures of both photocatalysts are distinctly different. While the B-TiO_2_350 °C_1.5 exhibits the presence of brookite, the reference sample

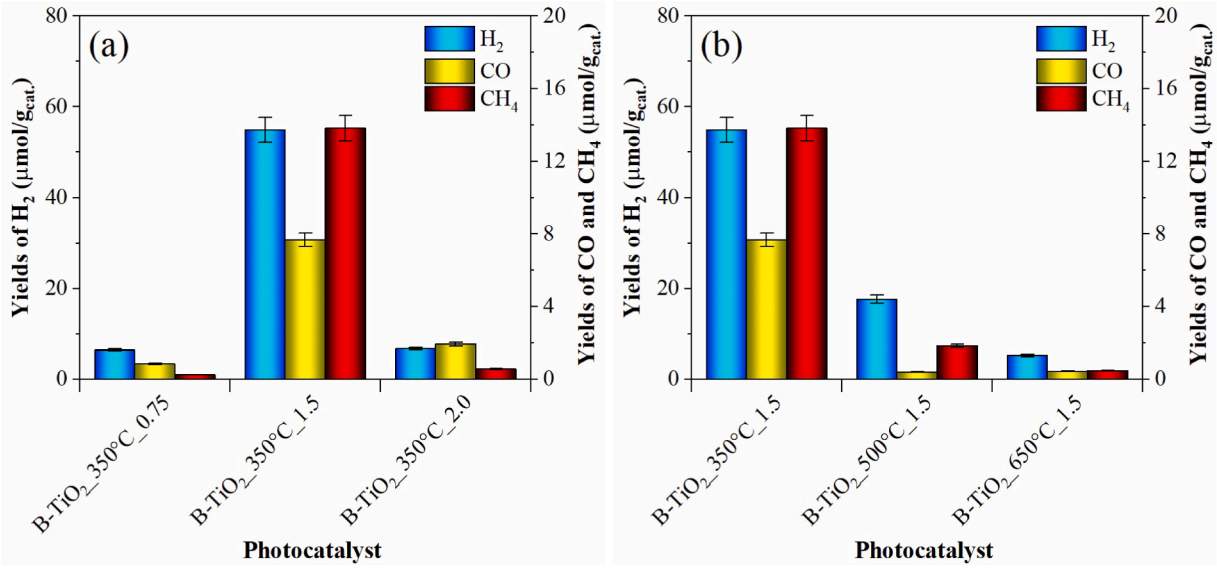

Fig. 1. Yields of the obtained products (H_2, CO, CH_4) after 7 h of CO_2 photoreduction over the investigated B-TiO_2 samples synthesized with different amounts of the reducing agent $NaBH_4$ (a) and reduced at different temperatures (b), with error bars indicating a measurement error within 5 %.

W-TiO_2_350 °C shows a mixed phase consisting of anatase and brookite.

Raman spectroscopy results confirmed that $NaBH_4$ reduction of the investigated TiO_2-based samples led to the successful formation of a disordered structure. This finding is evidenced by the characteristic hypsochromic shift of the main E_g Raman peak, indicative of the presence of crystalline TiO_2, in B-TiO_2-based samples to values ranging from 142 to 154 cm^{-1}, compared to the reference sample W-TiO_2_350 °C, which exhibited E_g peak with maximum at 139 cm^{-1} (Fig. 3a – c) [29,38]. The only exception is the B-TiO_2 sample calcined at 650 °C (B-TiO_2_650 °C), which exhibited negative shift to 134 cm^{-1}.

In addition, the Raman spectra of B-TiO_2-based samples reduced at 350 °C with 1.5 and 2.0 g of $NaBH_4$ (B-TiO_2_500 °C, B-TiO_2_650 °C), shown in Fig. 3a, confirm the presence of amorphous phase within these samples, as also indicated by the TEM and XRD results. This observation is further supported by the noticeable broadening of the detected Raman peaks, indicating a lack of long-range order in the structure of the samples [39,40].

Since the surface of photocatalysts plays a crucial role in the photocatalytic CO_2 reduction process, understanding the chemical composition of the surface structure is essential. To obtain these insights, XPS analysis was performed.

As shown in Figure S4, which displays the O 1 s XPS spectra of the investigated samples, all prepared photocatalysts exhibit XPS peaks at 530.1 eV, 531.1 eV, and 532.9 eV. These peaks are characteristic for lattice oxygen bonds (O_{Ti-O}), oxygen vacancies (O_v), and O-H group (O_{O-H}) [29,41,42]. Detailed quantitative analysis of detected oxygen species is provided in Table S1. XPS also detected Ti(IV) $2p_{1/2}$ and Ti(IV) $2p_{3/2}$ peaks at 464.4 and 458.6 eV, corresponding to the presence of Ti^{4+} species on the surface of the investigated photocatalyst samples (Figure S5) [43]. Additionally, as depicted in Figure S5, XPS measurements demonstrated the successful reduction of Ti^{4+} to Ti^{3+} active sites, confirmed by the Ti(III) $2p_{1/2}$ and Ti(III) $2p_{3/2}$ peaks at 463.0 and 457.4 eV [43–45].

Textural parameters are another key factor likely influencing the photocatalytic performance of the tested photocatalyst samples. At first glance, significant variations in specific surface area (S_{BET}) and total pore volume (TPV) across the investigated samples suggest that defect incorporation impacts the porosity of the materials. Based on the shape of the measured N_2 adsorption-desorption isotherms, which correspond to type IV as defined by the BDDT classification (Brunauer-Deming-Deming-Teller), the mesoporous nature of the prepared photocatalysts was revealed (Figure S6) [46]. This is also consistent with the calculated mesopore volume presented in Table 2. Additionally, further analysis of the measured data reveals two distinct trends. Namely, in the first trend, it is observed that an increase in the dose of $NaBH_4$ leads to a higher total pore volume, which in turn results in an increased specific surface area (Table 2). In the second trend, the data indicate that increasing the reduction temperature decreases both specific surface area and total pore volume (Table 2), induced by the annealing at higher temperatures, as well as an increase in particle size and the agglomeration of the titania samples [47].

Charge carrier separation is a critical step in the photocatalytic process. To explore and describe this aspect in detail, photoelectrochemical measurements were performed on the analyzed samples.

As shown in Figure S7, the reference sample W-TiO_2_350 °C generated the highest photocurrent response among all tested samples. In contrast, all reduced TiO_2-based photocatalysts (all B-TiO_2-based photocatalysts) exhibited significantly lower photocurrent compared to the reference sample (W-TiO_2_350 °C). This phenomenon can be attributed to the increased concentration of oxygen vacancies on the surface of the B-TiO_2-based photocatalyst samples.

The concentration of surface defects, such as oxygen vacancies, plays a key role in evaluating the photocatalytic activity of the prepared samples. The obtained XPS data (Table S1) and the photocurrent spectra (Figures S7 and S8) clearly reveal an inverse correlation between the generated photocurrent and the concentration of oxygen vacancies. A high concentration of surface oxygen vacancies in the tested samples appears to hinder transport of charge carriers, which is reflected in the reduced photocurrent response [48,49]. Wang et al. [50] even characterize these defects as energy bridges, which do not contribute to the transfer of charge carriers, but instead increase charge recombination.

Based on these findings, one might expect that the photocatalytic activity of the samples tested for CO_2 reduction should be diminished, as evidenced by the low photocurrent generation (Figures S7 and S8). However, while defects, such as oxygen vacancies, negatively impact photocurrent measurements, they do not necessarily hinder the photocatalytic activity of the samples. Indeed, the generated electrons can still be trapped by the introduced defects and subsequently interact with the adsorbed CO_2 during photocatalytic process to form products [29].

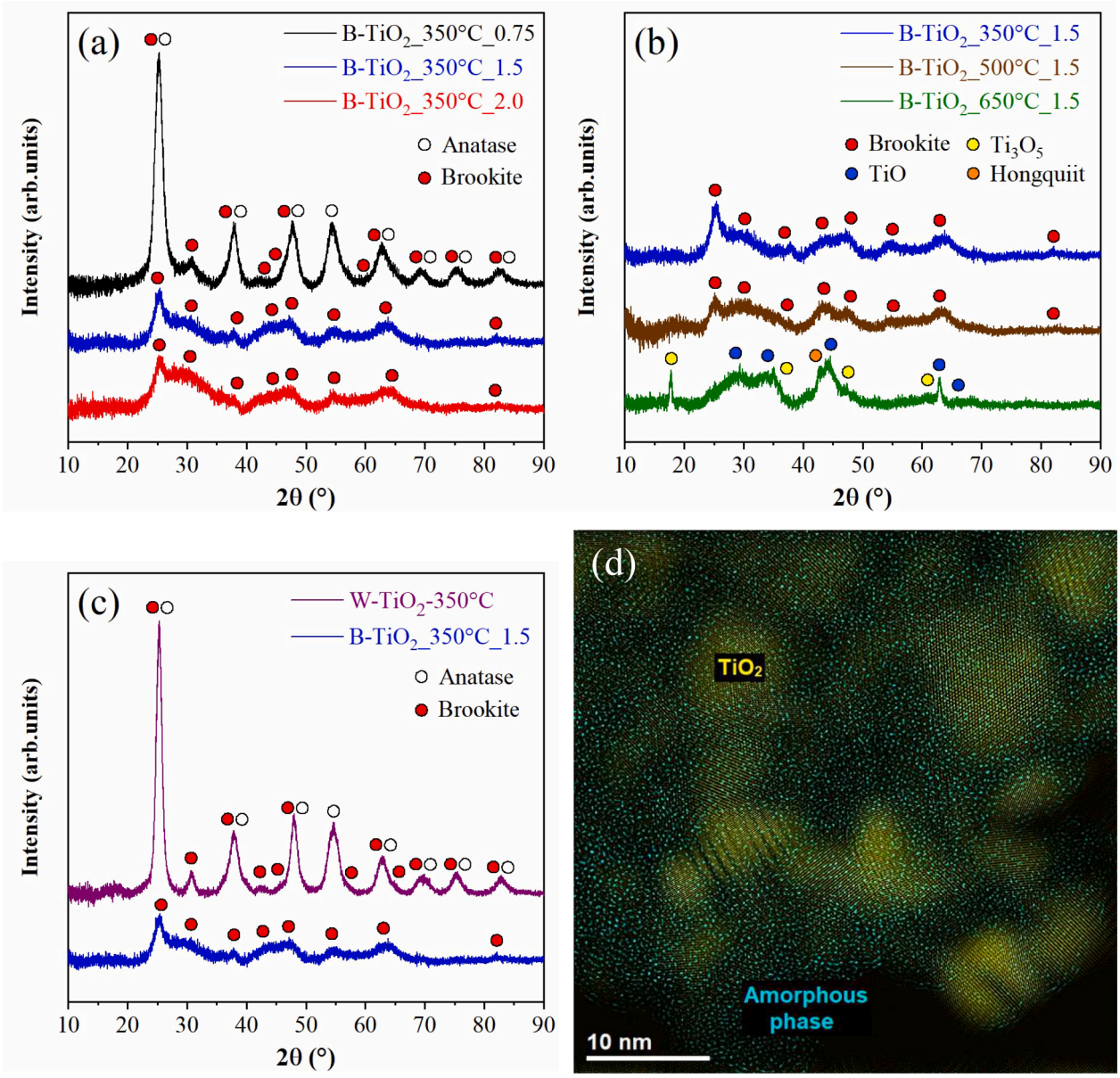

Fig. 2. XRD spectra of the investigated samples B-TiO_2-based samples under various reduction conditions: (a) samples reduced at 350 °C with varying amounts of $NaBH_4$ reducing agent (0.75 g, 1.5 g, 2.0 g), (b) samples reduced with 1.5 g of $NaBH_4$ reducing agent at three pre-selected temperatures (350 °C, 500 °C, 650 °C), (c) comparison between the XRD spectra of the most active B-TiO_2-based sample B-TiO_2_350 °C_1.5 and the reference sample W-TiO_2_350 °C, calcined at 350 °C, (d) coloured TEM image of the most active photocatalyst sample B-TiO_2_350 °C_1.5.

3.3. Correlation between physico-chemical properties and photocatalytic activity of investigated samples

A detailed analysis of the obtained data clearly confirmed that $NaBH_4$ dosage and reduction temperature are the key parameters primarily influencing the physico-chemical properties of the investigated photocatalysts, which in turn affect the efficiency of the CO_2 photoreduction process.

As shown in Fig. 1a, the variation in the amount of $NaBH_4$ reductant used during the chemical reduction significantly impacts the photocatalytic performance of the samples. Specifically, the photocatalytic performance appears to be driven by the presence of oxygen vacancies, which are an important part of the defect-rich structure of B-TiO_2-based samples.

The B-TiO_2 sample reduced with 1.5 g of $NaBH_4$ exhibited an optimal concentration of introduced Ti^{3+} sites and surface oxygen vacancies, which positively influenced its photocatalytic activity. Indeed, these defects can serve as active sites, facilitating the adsorption and activation of CO_2 molecules [24,51].

In contrast, the B-TiO_2 samples reduced with 0.75 g (B-TiO_2_350 °C_0.75) and 2.0 g (B-TiO_2_350 °C_2.0) of $NaBH_4$ showed a significant drop in photocatalytic activity compared to B-TiO_2_350 °C_1.5. As shown in Fig. 4, this behaviour is strongly connected to the variation in the Ti^{3+}/O_v ratio (Fig. 4, Table 3). The B-TiO_2_350 °C_0.75 sample reduced with 0.75 g of reducing agent exhibited an insufficient degree of $NaBH_4$ reduction, resulting in a low Ti^{3+}/O_v ratio and, consequently, reduced photocatalytic performance. On the other hand, the B-TiO_2_350 °C_2.0 sample, reduced at the same temperature but with 2.0 g of $NaBH_4$, also showed a decrease in the Ti^{3+}/O_v ratio (Fig. 4, Table 3) and, consequently, a low photocatalytic performance. In this case, the $NaBH_4$ reduction became too aggressive, causing undesirable stress on the TiO_2 lattice and destabilization of the crystal structure [52,53]. This resulted in a limited formation of effective defects and, therefore, a lower photocatalytic efficiency.

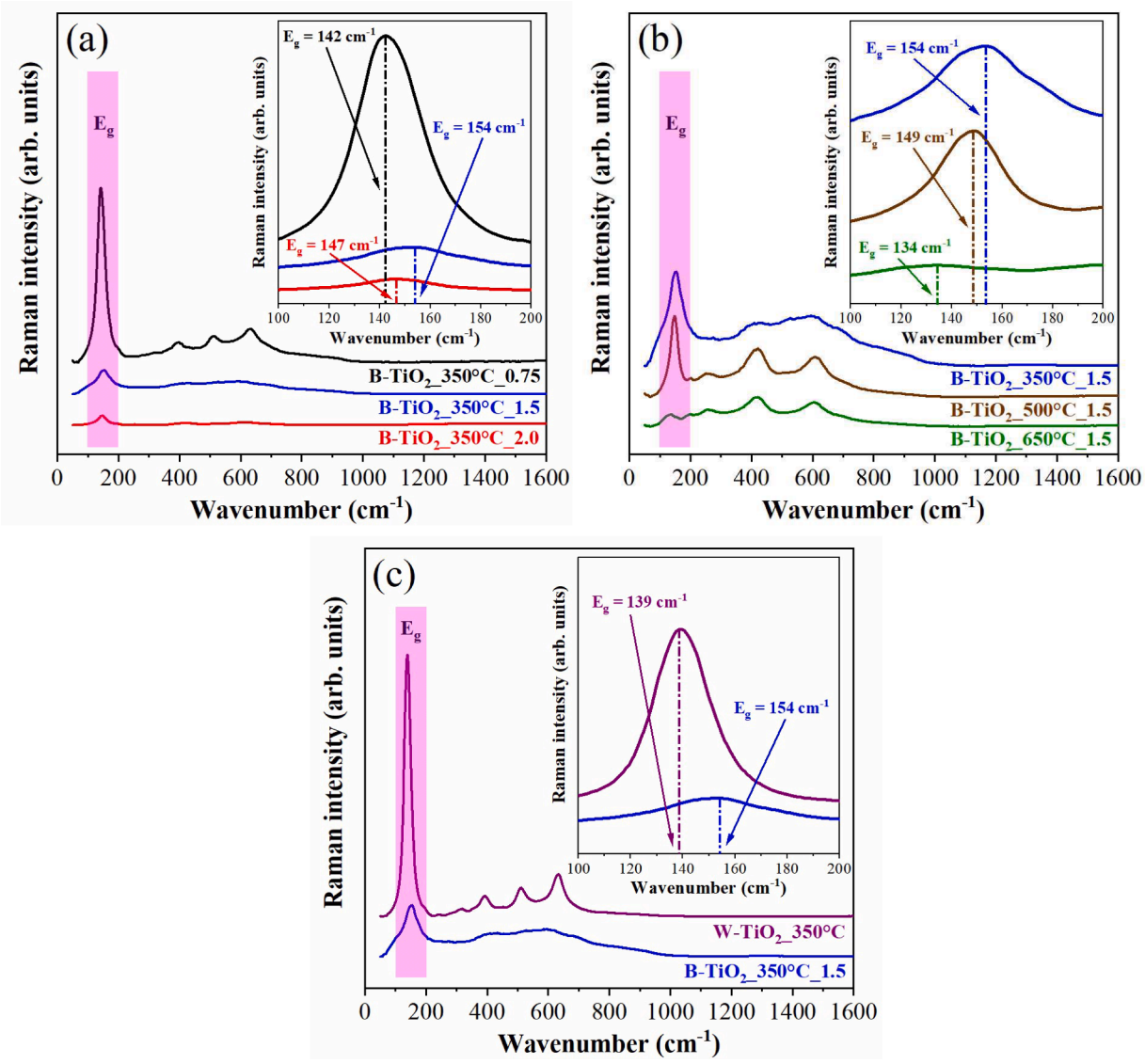

Fig. 3. Raman spectra highlighting the main E_g peak of the investigated samples: (a) B-TiO_2 reduced at 350 °C with 0.75, 1.5, and 2.0 g of $NaBH_4$ reductant, (b) B-TiO_2 reduced at 350 °C, 500 °C, and 650 °C with 1.5 g of $NaBH_4$ reducing agent, (c) comparison between the most active B-TiO_2-based sample, B-TiO_2_350 °C_1.5, and the prepared reference sample W-TiO_2_350 °C.

Table 2
Textural parameters of the investigated photocatalyst samples.

Sample	S_{BET} (m^2/g)	TPV (cm^3/g) [a]	V_{micro} (cm^3/g) [b]	V_{meso} (cm^3/g) [c]
B-TiO_2_350 °C_0.75	134	0.159	0.052	0.107
B-TiO_2_350 °C_1.5	153	0.170	0.059	0.111
B-TiO_2_350 °C_2.0	193	0.218	0.067	0.151
B-TiO_2_500 °C_1.5	70	0.134	0.026	0.108
B-TiO_2_650 °C_1.5	40	0.084	0.015	0.069
W-TiO_2_350 °C	142	0.317	0.050	0.267

[a] … Total pore volume.
[b] … Volume of micropores (determined using the Dubinin-Radushkevich equation).
[c] … Volume of mesopores (calculated from the difference of TPV and V_{micro}).

Samples calcined at higher temperatures (400 °C and above) also exhibited reduced activity, likely due to defect deactivation and increased surface hydroxylation, as discussed further in the following discussion.

The crucial role of Ti^{3+} sites in enhancing photocatalytic activity underscores is further supported by the corresponding Ti^{3+}/Ti^{4+} ratios (Table 3). As illustrated in Fig. 5, an increasing concentration of surface Ti^{3+} sites correlate with improved photocatalytic efficiency. These Ti^{3+} centers, in combination with oxygen vacancies, promote the adsorption and activation of CO_2 molecules [29,31]. Furthermore, they introduce localized electronic states that act as electron traps, effectively suppressing the recombination of photogenerated charge carriers and stabilizing electrons for subsequent CO_2 photoreduction [54].

The previous paragraphs clearly highlight the positive role of oxygen vacancies and Ti^{3+} active sites in the photocatalytic CO_2 reduction of the prepared defect-rich TiO_2-based samples. However, the crucial role of $O_{O\text{-}H}$ groups, detected on the surface of the investigated photocatalysts by XPS analysis, should not be overlooked. In particular, $O_{O\text{-}H}$ groups may contribute to enhanced adsorption of CO_2 molecules [55] or participate in proton transfer processes essential for the reduction of CO_2 to hydrocarbons [56]. Nevertheless, an excessive concentration of $O_{O\text{-}H}$

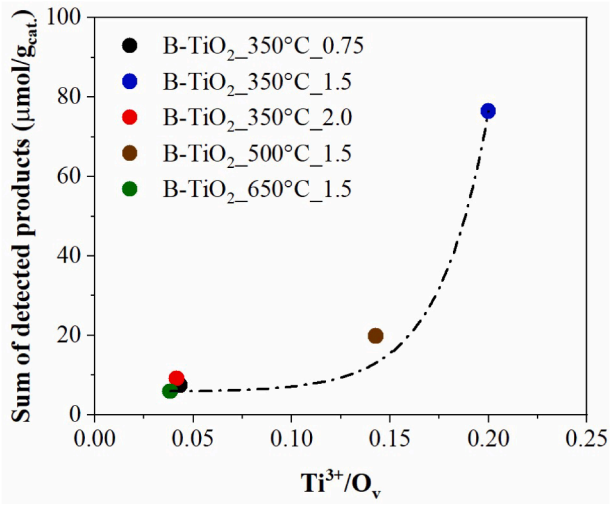

Fig. 4. Correlation between the total yields of all products and the oxygen vacancies.

Table 3
Determined ratios of crucial Ti^{3+} and oxygen-based species obtained from analysis of O 1 s and Ti 2p high-resolution XPS spectra and the total product yields of photocatalytic products for the reduced photocatalysts.

Sample	Ti^{3+}/O_v	Ti^{3+}/Ti^{4+}	$Ti^{3+}/O_{O—H}$	Sum of detected products ($\mu mol/g_{cat.}$)
B-TiO_2_350 °C_0.75	0.04	0.01	0.11	7.46
B-TiO_2_350 °C_1.5	0.20	0.05	0.36	76.39
B-TiO_2_350 °C_2.0	0.04	0.01	0.05	9.18
B-TiO_2_500 °C_1.5	0.14	0.04	0.20	19.82
B-TiO_2_650 °C_1.5	0.04	0.01	0.04	5.91

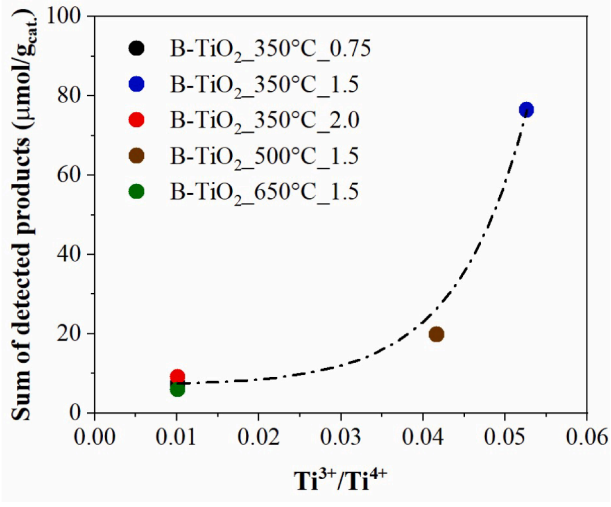

Fig. 5. Correlations between the sum of the yields of all products and determined Ti^{3+}/Ti^{4+} ratios.

groups can also inhibit the photocatalytic process by trapping photogenerated electrons or by blocking active sites. This phenomenon is observable for the B-TiO_2 sample reduced at 650 °C, where the photocatalytic activity declined due to the highest proportion of hydroxyl groups relative to surface oxygen vacancies, while the amount of lattice oxygen decreased (Table 4). This may indicate excessive surface hydroxylation. In other words, most of the oxygen vacancies become saturated with hydroxyl groups, which led to their passivation and a loss of active centres for the photocatalytic process. Notably, only the B-TiO_2 sample reduced at the lowest preselected temperature (350 °C) exhibited the highest photocatalytic activity for CO_2 reduction. This suggests that a favourable balance between introduced surface oxygen vacancies and hydroxyl groups was achieved only in this photocatalyst (B-TiO_2_350 °C_1.5).

As depicted in Fig. 6, the photocatalytic performance during CO_2 photoreduction of the investigated defect-rich B-TiO_2 samples was strongly influenced by the ratio of introduced Ti^{3+} active sites to hydroxyl groups. Specifically, the B-TiO_2 sample reduced at 350 °C with 1.5 g of $NaBH_4$ exhibited the highest ratio of Ti^{3+} sites to $O_{O\text{-}H}$ groups and, consequently, the highest CO_2 photoreduction performance. Conversely, the photocatalysts synthesized with 0.75 g and 2.0 g of $NaBH_4$ showed the opposite trend. A significant decrease in the $Ti^{3+}/O_{O\text{-}H}$ ratio was observed along with a drop in photocatalytic activity for CO_2 photoreduction. A similar trend was observed with increasing reduction temperature to 500 °C and 650 °C, which also led to a decline in both $Ti^{3+}/O_{O—H}$ ratio and the overall photocatalytic activity. Based on these insights, it should be underscored that achieving a balanced concentration not only between oxygen vacancies and $O_{O\text{-}H}$ groups, but also between Ti^{3+} active sites and $O_{O\text{-}H}$ groups, is crucial for optimizing photocatalytic performance.

Furthermore, a detailed analysis of the obtained data revealed significant differences in the photoactivity for CO_2 photoreduction and selectivity, which was calculated using Eqs. (4) and 5. As shown in Fig. 7a, within the B-TiO_2 series of samples prepared with different amounts of reducing agent, the sample B-TiO_2_350 °C reduced with 1.5 g $NaBH_4$ exhibited the highest selectivity towards CH_4. This can be attributed to the optimal combination of defects (Ti^{3+} and O_v) and partial hydroxylation. At a lower load (0.75 g), the reduction was insufficient and fewer effective defects are formed, which led to lower selectivity towards CH_4 and simultaneously higher CO production. In contrast, 2.0 g of $NaBH_4$ caused excessive reduction and a decrease in the number of active sites (defects), which reflected in a decrease in selectivity towards CH_4 and, conversely, an increase in selectivity towards CO.

Based on the available data, it was also confirmed, that increase in surface hydroxylation occurred mainly in B-TiO_2_500 °C and B-TiO_2_650 °C samples. Hydroxyl groups promote protonation and thus CH_4 formation, which explains their slightly higher selectivity for this product. However, at higher degrees of hydroxylation, partial passivation of the surface and a reduction in CO_2 adsorption may occur, resulting in a decrease in photocatalytic performance. A balance between defect sites and hydroxyl surface groups is therefore critical for high photoactivity (Fig. 7b).

Table 4
Detailed analysis of surface oxygen species and the $O_{O—H}/O_v$ ratio in reduced B-TiO_2 samples based on O 1 s high-resolution XPS spectra.

Sample	Oxygen lattice (%)	Oxygen vacancies (%)	Hydroxyl groups (%)	$O_{O—H}/O_v$
B-TiO_2_350 °C_0.75	68	23	9	0.39
B-TiO_2_350 °C_1.5	61	25	14	0.56
B-TiO_2_350 °C_2.0	57	24	19	0.79
B-TiO_2_500 °C_1.5	52	28	20	0.71
B-TiO_2_650 °C_1.5	46	26	28	1.08

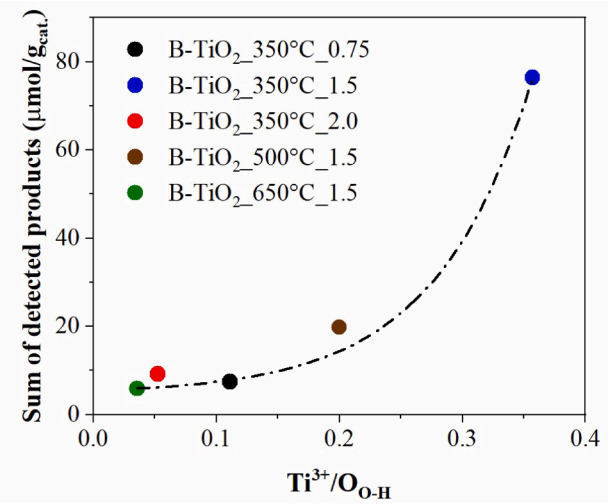

Fig. 6. Correlations between the yields of carbonaceous products and the ratio of Ti^{3+} sites and detected hydroxyl groups for B-TiO_2 reduced with different amounts of $NaBH_4$ reductant and temperature.

$$\text{Selectivity for CO} = \frac{[2r(CO)]}{[2r(CO) + 8r(CH_4) + 2r(H_2)]} \cdot 100\% \quad (4)$$

$$\text{Selectivity for } CH_4 = \frac{[8r(CH_4)]}{[2r(CO) + 8r(CH_4) + 2r(H_2)]} \cdot 100\% \quad (5)$$

Where $r(H_2)$, $r(CH_4)$ and $r(CO)$ are formation rates of H_2, CH_4 and CO.

Notably, the defect-based B-TiO_2 sample, reduced at 350 °C with 1.5 g of $NaBH_4$ reductant (B-TiO_2_350 °C_1.5), exhibits not only a significantly higher photocatalytic performance for CO_2 photoreduction (Fig. 8a, Figure S9a – c), but also higher selectivity compared to the prepared reference sample W-TiO_2_350 °C and the commercially available TiO_2 – P25 (Fig. 8b).

The selectivity for CO_2 photoreduction was calculated by using the following formula (Eq. (6)) [37,57]:

$$\text{Selectivity for } CO_2 \text{ reduction} = \frac{[2r(CO) + 8r(CH_4)]}{[2r(CO) + 8r(CH_4) + 2r(H_2)]} \cdot 100\% \quad (6)$$

The results of the photocatalytic tests clearly emphasize the beneficial effect of a defective structure on CO_2 photoconversion. This finding is supported by the data presented in Fig. 8. These indicate that the defect-rich TiO_2 sample, B-TiO_2_350 °C_1.5, exhibits significantly higher photocatalytic activity than both the prepared reference TiO_2 sample, W-TiO_2_350 °C, and the commercial TiO_2 – P25, both of which lack a high concentration of surface defects.

This superior performance can be primarily attributed to the synergistic effect of Ti^{3+} active sites and oxygen vacancies, along with their balanced concentration towards the hydroxyl groups. Based on these observations, it is clear that the presence of these defects (Ti^{3+} active sites and oxygen vacancies) in B-TiO_2_350 °C_1.5 sample enhances the activation and conversion of CO_2 molecules into other products. This distinction significantly sets it apart from the counterparts with a non-defect-rich structure, such as W-TiO_2_350 °C and P25 in this case, thereby highlighting the importance of defect engineering in the field of photocatalysis (Fig. 8).

Based on experimental results, only CO and CH_4 were detected as carbonaceous products of CO_2 photoreduction. This observation suggests that the reaction most likely proceeds via a direct multi-electron reduction pathway, corresponding to two-electron (CO formation) and eight-electron (CH_4 formation) reduction processes. Although the presence of surface-bound intermediates such as formate (HCOO)* or carboxyl-(COOH)* species cannot be completely ruled out [58–60], but no experimental evidence for these species was obtained in this study. Therefore, the photoreduction of CO_2 on defective TiO_2 can be attributed to a direct multi-electron mechanism facilitated by defects (Ti^{3+} sites and O_v) that promote the adsorption, activation, and subsequent CO_2 photoreduction.

4. Conclusions

This work highlights the pivotal role of defect engineering in tuning the photocatalytic performance of TiO_2-based materials for CO_2 reduction. The sol–gel synthesis combined with $NaBH_4$ reduction successfully introduced a controlled amounts of surface defects, particularly oxygen

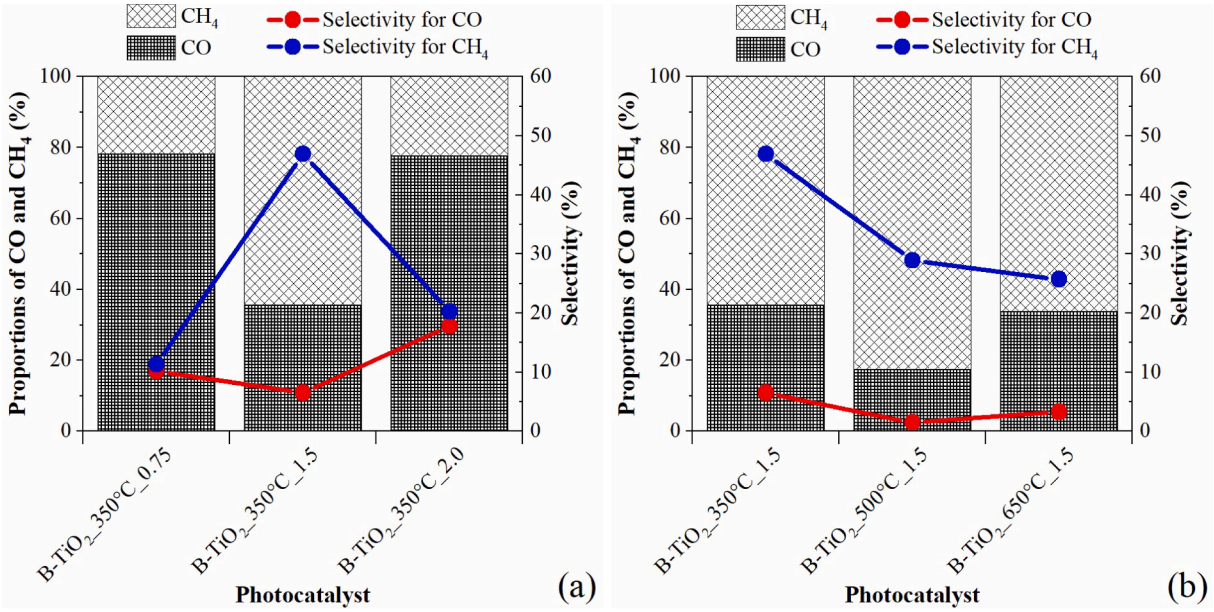

Fig. 7. Carbon-based product distribution (CO and CH_4) and corresponding selectivities during CO_2 photoreduction over B-TiO_2 photocatalysts: (a) photocatalysts prepared at 350 °C using different amounts of $NaBH_4$ reducing agent and (b) samples prepared with 1.5 g $NaBH_4$, but at different reduction temperatures.

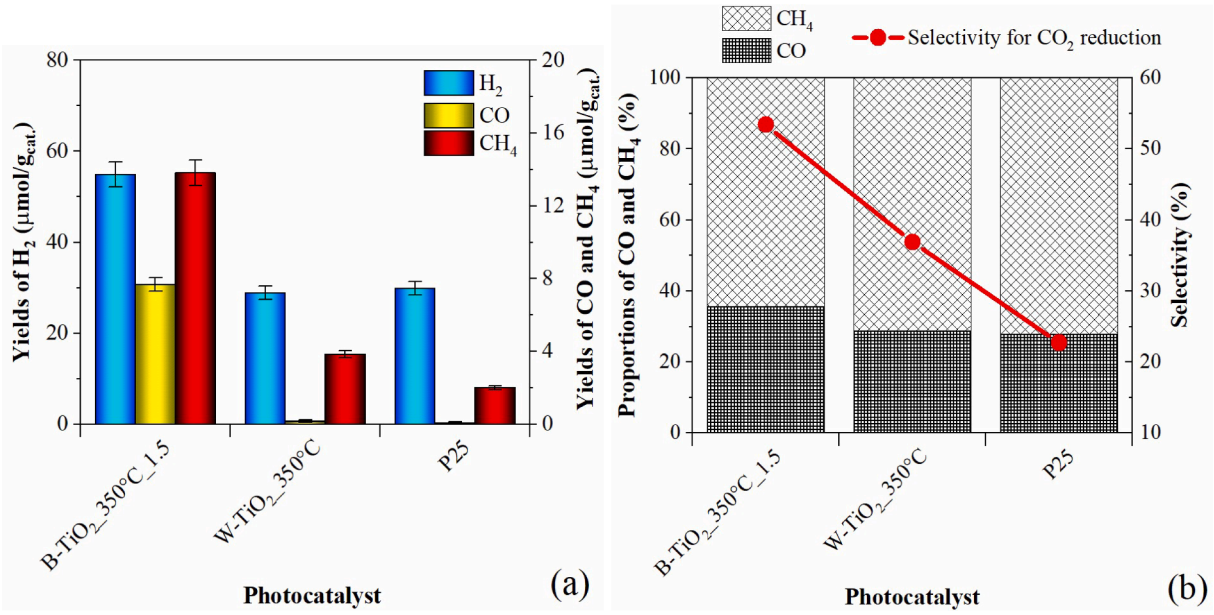

Fig. 8. a) Yields of the obtained H_2 CO, CH_4 and b) proportions of CO and CH_4 yields after 7 h of CO_2 photoreduction in the presence of the most active B-TiO_2-based sample, B-TiO_2_350 °C_1.5, compared to the reference samples W-TiO_2_350 °C and commercial TiO_2 – P25.

vacancies and Ti^{3+} species. Among the tested photocatalysts, the sample reduced at 350 °C with 1.5 *g* $NaBH_4$ demonstrated superior CO_2 photoreduction efficiency and selectivity toward CH_4 and CO, outperforming both a reference defect-poor TiO_2 and commercial TiO_2–P25. The enhanced activity is attributed to the synergistic effect of oxygen vacancies and Ti^{3+}centers, coupled with an optimal concentration of surface hydroxyl groups that facilitate CO_2 adsorption and electron transfer. The study reveals that both the amount of reductant and the reduction temperature are key parameters that dictate defect formation and stability. Importantly, an excessive number of defects or thermal treatment can lead to structural destabilization or recombination losses. Thus, achieving a balance between Ti^{3+}, oxygen vacancies, and hydroxyl groups is crucial for maximizing photocatalytic performance.

CRediT authorship contribution statement

Rudolf Ricka: Writing – review & editing, Writing – original draft, Visualization, Validation, Methodology, Investigation, Conceptualization. **Agnieszka Wanag:** Writing – review & editing, Writing – original draft, Methodology, Investigation. **Ewelina Kusiak-Nejman:** Writing – review & editing, Writing – original draft, Supervision, Conceptualization. **Martin Reli:** Writing – review & editing, Writing – original draft, Investigation. **Miroslava Filip Edelmannová:** Writing – review & editing, Writing – original draft, Investigation. **Marcin Łapinski:** Writing – review & editing, Writing – original draft, Investigation. **Grzegorz Słowik:** Writing – review & editing, Writing – original draft, Investigation. **Antoni W. Morawski:** Writing – review & editing, Writing – original draft, Supervision, Methodology, Conceptualization. **Kamila Kočí:** Writing – review & editing, Writing – original draft, Supervision, Conceptualization.

Declaration of competing interest

The authors declare that they have no known competing financial interests or personal relationships that could have appeared to influence the work reported in this paper.

Acknowledgements

This research was supported by the Large Research Infrastructure ENREGAT (project No LM2023056), Norway Grants 2014–2021 via the National Centre for Research and Development (grant No NOR/ POL-NORCCS/PhotoRed/0007/2019–00), the project „Waste as an alternative source of energy“, reg. nr. CZ.02.01.01/00/23_021/0008590 under the Programme Johannes Amos Comenius, European Unionś Horizon Europe project SAN4Fuel (Grant No HORIZON-WIDERA-2021-ACCESS-03–01: 101079384), European Union under the REFRESH - Research Excellence For Region Sustainability and High-tech Industries (project No CZ.10.03.01/00/22_003/0000048) via the Operational Programme Just Transition, and the grant programme “Support for Science and Research in the Moravia-Silesia Region 2022″ (RRC/12/2022).

During the preparation of this work the author(s) used ChatGPT solely for language editing purposes. After using this tool, the author(s) reviewed and edited the content as needed and take(s) full responsibility for the content of the publication.

Supplementary materials

Supplementary material associated with this article can be found, in the online version, at doi:10.1016/j.apsadv.2025.100925.

Data availability

FAIR principles will be available after manuscript acceptance on Zenodo: 10.5281/zenodo.16811745.

References

[1] N. Smigic, I. Djekic, N. Tomic, B. Udovicki, A. Rajkovic, The potential of foods treated with supercritical carbon dioxide (sc-CO_2) as novel foods, Br. Food J. 121 (2019) 815–834.
[2] V. Reyes, E. Cahill, K.E. Mis Solval, The potential for reducing food waste through shelf-life extension: actionable insights from data digitization, Sustainability 16 (2024) 2986.
[3] X. Sun, Y.V. Fan, Y. Lei, J. Zhao, W. Chen, Z. Cao, Towards decoupling in chemical industry: input substitution impacted by technological progress, J Clean Prod 452 (2024) 142040.
[4] NASA, Carbon dioxide, in: S.C. Editors (Ed.), 2024.

[5] L. Xiao, S. Gao, R. Liao, Y. Zhou, Q. Kong, G. Hu, C_3N_5-based nanomaterials and their applications in heterogeneous catalysts, energy harvesting, and environmental remediation, Mater Horiz 11 (2024) 2545–2571.

[6] S. Gomey, E. Guliani, K. Choudhary, S. Sengupta, B. Chakraborty, M. Raula, Photoactive metal chalcogenides towards CO_2 reduction–a review, Colloid Polym Sci 302 (2024) 1149–1167.

[7] K. Zhong, P. Sun, H. Xu, Advances in defect engineering of metal oxides for photocatalytic CO2 reduction, Small, n/a 2310677.

[8] R. Mori, CO_2 photocatalytic reduction with robust and stable metal–organic framework: a review, Mater. Renew. Sustain. Energy 13 (2024) 109–132.

[9] W. Xu, Y. Peng, D. Hu, I. Razanau, D. Gu, W. Xiao, Molten salt synthesis of Ti3C2/Cu cocatalyst for enhanced TiO2 photocatalytic CO2 reduction, ChemCatChem, n/a e202400873.

[10] M.d.l.M. Ballari, M. Filip Edelmannová, R. Ricka, M. Reli, K. Kočí, Exploring kinetics and mass transfer in photocatalytic CO_2 reduction: impact of photocatalyst loading and stirrer speed, Energy Convers. Manag.: X 23 (2024) 100651.

[11] R. Ricka, T.W.M. Amen, N. Tsunoji, M. Reli, M. Filip Edelmannová, M. Kormunda, M. Ritz, K. Kočí, Titanium-immobilized layered HUS-7 silicate as a catalyst for photocatalytic CO2 reduction, ChemSusChem, n/a e202400434.

[12] Z. Pan, M. Liu, P. Niu, F. Guo, X. Fu, X. Wang, Photocatalytic CO_2 reduction using Ni_2P nanosheets, Acta Phys.-Chim. Sin. 36 (2020) 1906014.

[13] D. Zhao, X. Tang, P. Liu, Q. Huang, T. Li, L. Ju, Recent progress of ion-modified TiO_2 for enhanced photocatalytic hydrogen production, Molecules 29 (2024) 2347.

[14] J. Chen, T. Li, X. An, D. Fu, Photocatalytic reduction of CO_2 by TiO_2 modified materials: recent advances and outlook, Energy Fuels 38 (2024) 7614–7636.

[15] B. Zhang, B. Sun, F. Liu, T. Gao, G. Zhou, TiO_2-based S-scheme photocatalysts for solar energy conversion and environmental remediation, Sci. China Mater. 67 (2024) 424–443.

[16] K. Qi, C. Imparato, O. Almjasheva, A. Khataee, W. Zheng, TiO_2-based photocatalysts from type-II to S-scheme heterojunction and their applications, J Colloid Interface Sci 675 (2024) 150–191.

[17] R. Ricka, A. Wanag, E. Kusiak-Nejman, D. Moszyński, M.F. Edelmannová, M. Reli, Z. Baďura, G. Zoppellaro, R. Zbořil, A.W. Morawski, K. Kočí, Photocatalytic reduction of CO_2 over Ti^{3+} self-doped TiO_2-based nanomaterials, J. CO2 Util. 80 (2024) 102701.

[18] A.-Y. Lo, C.-C. Wang, J. Huang, Y.-C. Chung, Y.-C. Chang, Defect-synergetic effect enhanced CO_2 photoreduction efficiency of TiO_2 nanostructures with Fe dopants, J. Environ. Chem. Eng. 12 (2024) 112351.

[19] M. Tahir, Constructing solid waste-derived carbon fiber with self-doped Ti^{3+}/TiO_2 ($SWCFs/Ti^{3+}/TiO_2$) heterojunction for photocatalytic CO2 reduction, Clean Technol. Environ. Policy (2024).

[20] W. Saputera, A. Satriyatama, I. Budi, A. Saputro, M. Mahyuddin, W. Utomo, S. Mutiara, H. Chung, Arramel, F. Abdi, D. Sasongko, Understanding the role of copper oxidation State on a TiO_2/ZSM-5 catalyst for photocatalytic CO_2 reduction to methanol, Adv Mater Interfaces 12 (2025).

[21] X. Hou, Y. Li, H. Zhang, P.D. Lund, J. Kwan, S.C.E. Tsang, Black titanium oxide: synthesis, modification, characterization, physiochemical properties, and emerging applications for energy conversion and storage, and environmental sustainability, Chem Soc Rev 53 (2024) 10660–10708.

[22] S. Akrami, M. Watanabe, T.H. Ling, T. Ishihara, M. Arita, M. Fuji, K. Edalati, High-pressure TiO_2-II polymorph as an active photocatalyst for CO_2 to CO conversion, Appl. Catal. B: Environ. 298 (2021) 120566.

[23] S. Akrami, Y. Murakami, M. Watanabe, T. Ishihara, M. Arita, M. Fuji, K. Edalati, Defective high-entropy oxide photocatalyst with high activity for CO_2 conversion, Appl. Catal. B: Environ. 303 (2022) 120896.

[24] M. Katai, P. Edalati, J. Hidalgo-Jimenez, Y. Shundo, T. Akbay, T. Ishihara, M. Arita, M. Fuji, K. Edalati, Black brookite rich in oxygen vacancies as an active photocatalyst for CO_2 conversion: experiments and first-principles calculations, J. Photochem. Photobiol. A: Chem. 449 (2024) 115409.

[25] M. Kitchin, K. Konstas, C.J. Sumby, M.L. Czyz, P. Valente, M.R. Hill, A. Polyzos, C. J. Doonan, Continuous flow synthesis of a carbon-based molecular cage macrocycle via a three-fold homocoupling reaction, Chem. Commun. 51 (2015) 14231–14234.

[26] A. Raes, A.C. Minja, K.R. Ag, S.W. Verbruggen, Recent advances in metal-doped defective TiO_2 for photocatalytic CO_2 conversion, Curr Opin Chem Eng 44 (2024) 101013.

[27] L. Shen, Z. Xie, L. Hou, J. Yang, Q. Li, Synthesis of a defective WO_{3-y}/TiO_{2-x} composite catalyst for photocatalytic CO_2 highly selective reduction, Energy Fuels 36 (2022) 11515–11523.

[28] X. Qian, W. Yang, S. Gao, J. Xiao, S. Basu, A. Yoshimura, Y. Shi, V. Meunier, Q. Li, Highly selective, defect-induced photocatalytic CO_2 reduction to acetaldehyde by the Nb-doped TiO_2 nanotube array under simulated solar illumination, ACS Appl Mater Interfaces 12 (2020) 55982–55993.

[29] R. Ricka, A. Wanag, E. Kusiak-Nejman, M. Filip Edelmannová, M. Reli, M. Łapinski, G. Słowik, A.W. Morawski, K. Kočí, Defective TiO_2 for CO_2 photoreduction: influence of alkaline agent and reduction temperature modulation, Catal Today 448 (2025) 115162.

[30] T.K. Rahul, M. Mohan, N. Sandhyarani, Enhanced solar hydrogen evolution over In situ gold–Platinum bimetallic nanoparticle-loaded Ti^{3+} self-doped titania photocatalysts, ACS Sustain Chem Eng 6 (2018) 3049–3059.

[31] Y. Zhang, Y. Wang, Z. Hu, J. Huang, S. Yang, H. Li, High-efficiency photocatalytic CO_2 reduction enabled by interfacial O_v and isolated Ti^{3+} of g-C_3N_4/TiO_2 Z-scheme heterojunction, J Colloid Interface Sci 663 (2024) 891–901.

[32] Z. Wang, R. Cai, Y. Zhang, X. Huang, Y. Bi, Dynamic crystal-structure and active-site of defective ZnAl-catalysts during CO_2 photoreduction, Angew. Chem. Int. Ed. 64 (2025) e202502834.

[33] J. Cai, H. Wang, H. Li, K. Li, High-performance photocatalytic reduction of CO_2 to CO by defective g-C_3N_4/CeO_2 under sacrificial agent-free conditions, J. Rare Earths 43 (2025) 1882–1891.

[34] M. Duflot, C. Marchal, V. Artero, K. Christoforidis, V. Keller, Modulation of NH_2-UiO-66 based MOFs for gas phase CO_2 photocatalytic reduction, Adv Energy Mater 15 (2025).

[35] J. Di, G. Hao, G. Liu, J. Zhou, W. Jiang, Z. Liu, Defective materials for CO_2 photoreduction: from C_1 to C_{2+} products, Coord Chem Rev 482 (2023) 215057.

[36] Y.A. Alli, P.O. Oladoye, A.T. Onawole, H. Anuar, S. Adewuyi, O.D. Ogunbiyi, K. Philippot, Photocatalysts for CO_2 reduction and computational insights, Fuel 344 (2023) 128101.

[37] M. Reli, P. Nadrah, M. Filip Edelmannová, R. Ricka, A. Sever Škapin, U. Lavrenčič Štangar, K. Kočí, Photocatalytic CO_2 reduction over mesoporous TiO_2 photocatalysts, Mater Sci Semicond Process 169 (2024) 107927.

[38] T.T. Nguyen, T.M. Cao, H.V. Le, V.V. Pham, Investigation of some characterizations of black TiO_2 nanotubes via spectroscopic methods, Commun. Phys. 29 (2019) 189.

[39] M.A. Vargas, J.E. Rodríguez-Páez, Amorphous TiO_2 nanoparticles: synthesis and antibacterial capacity, J Non Cryst Solids 459 (2017) 192–205.

[40] Z. Li, Y. Zhu, J. Wang, Q. Guo, J. Li, Size-controlled synthesis of dispersed equiaxed amorphous TiO_2 nanoparticles, Ceram Int 41 (2015) 9057–9062.

[41] D. Yao, Z. Hu, R. Zheng, J. Li, L. Wang, X. Yang, W. Lü, H. Xu, Black TiO_2-based dual photoanodes boost the efficiency of quantum dot-sensitized solar cells to 11.7%, Nanomaterials 12 (2022) 4294.

[42] D. Xiong, W. Li, L. Liu, Vertically aligned porous nickel(II) hydroxide nanosheets supported on carbon paper with long-term oxygen evolution performance, Chem. – Asian J. 12 (2017) 543–551.

[43] Y. Yang, P. Gao, X. Ren, L. Sha, P. Yang, J. Zhang, Y. Chen, L. Yang, Massive Ti^{3+} self-doped by the injected electrons from external Pt and the efficient photocatalytic hydrogen production under visible-light, Appl. Catal. B: Environ. 218 (2017) 751–757.

[44] J. Kuang, Z. Xing, J. Yin, Z. Li, S. Tan, M. Li, J. Jiang, Q. Zhu, W. Zhou, Ti^{3+} self-doped rutile/anatase/TiO_2(B) mixed-crystal tri-phase heterojunctions as effective visible-light-driven photocatalysts, Arab. J. Chem. 13 (2020) 2568–2578.

[45] B. Bharti, S. Kumar, H.-N. Lee, R. Kumar, Formation of oxygen vacancies and Ti^{3+} state in TiO_2 thin film and enhanced optical properties by air plasma treatment, Sci Rep 6 (2016) 32355.

[46] L. Liu, X. Gu, C. Sun, H. Li, Y. Deng, F. Gao, L. Dong, In situ loading of ultra-small Cu_2O particles on TiO_2 nanosheets to enhance the visible-light photoactivity, Nanoscale 4 (2012) 6351–6359.

[47] L. Andronic, D. Ghica, M. Stefan, C.G. Mihalcea, A.-M. Vlaicu, S. Karazhanov, Visible-light-active black TiO_2 nanoparticles with efficient photocatalytic performance for degradation of pharmaceuticals, Nanomaterials 12 (2022) 2563.

[48] Y. Zhao, S. Balasubramanyam, R. Sinha, R. Lavrijsen, M.A. Verheijen, A.A. Bol, A. Bieberle-Hütter, Physical and chemical defects in WO_3 thin films and their impact on photoelectrochemical water splitting, ACS Appl. Energy Mater. 1 (2018) 5887–5895.

[49] H. Chen, J. Li, W. Yang, S.E. Balaghi, C.A. Triana, C.K. Mavrokefalos, G.R. Patzke, The role of surface states on reduced TiO_2@$BiVO_4$ photoanodes: enhanced water oxidation performance through improved charge transfer, ACS Catal 11 (2021) 7637–7646.

[50] T. Wang, L. Xu, Z. Wu, Y. Li, Z. Yin, J. Han, Z. Yang, J. Qiu, Z. Song, Self-doping induced oxygen vacancies and lattice strains for synergetic enhanced upconversion luminescence of Er^{3+} ions in 2D BiOCl nanosheets, Nanoscale 14 (2022) 12909–12917.

[51] X. Yan, C. Duan, S. Yu, B. Dai, C. Sun, H. Chu, Revealing the mechanism of oxygen vacancy defect for CO_2 adsorption and diffusion on CaO: DFT and experimental study, J. CO2 Util. 79 (2024) 102648.

[52] S.A. Sabinas-Hernández, J.M. Gracia Jiménez, N.R. Silva González, M.P. Elizalde-González, U. Salazar-Kuri, S. Tehuacanero-Cuapa, Blue Titania: the outcome of defects, crystalline-disordered core-shell structure, and hydrophilicity change, Nanomaterials 12 (2022) 1501.

[53] Y. Yan, H. Yang, Z. Yi, T. Xian, $NaBH_4$-reduction induced evolution of Bi nanoparticles from BiOCl nanoplates and construction of promising Bi@BiOCl hybrid photocatalysts, Catalysts 9 (2019) 795.

[54] Y. Wang, X. Liu, K. Yu, Z. Ning, Q. Song, H. Xie, Ultra-fast synthesis of the high performance photocatalytic Ti^{3+} self-doped strontium titanate by an electrochemical assist in molten salt: effect of electrochemical potential, J. Mater. Chem. A 12 (2024) 6087–6092.

[55] H. Zhang, S. Gao, H. Guan, W. Yang, Q. Li, Highly selective photocatalytic CO_2 reduction to ethylene in pure water by Nb_2O_5 nanoparticles with enriched surface –OH groups under simulated solar illumination, J. Adv. Ceram. 12 (2023) 1641–1654.

[56] S. Sun, P. Gao, Y. Shen, T. Wu, Q. An, Enhanced water dissociation promotes photocatalytic CO_2 hydrogenation to methane: a case study of Pt-loaded MoO_3 catalyst, ACS Sustain Chem Eng 12 (2024) 14760–14770.

[57] B.T. Barrocas, J. Přech, M. Filip Edelmannová, E. Szaniawska, K. Kočí, J. Čejka, Titanosilicates enhance carbon dioxide photocatalytic reduction, Appl. Mater. Today 26 (2022) 101392.

[58] S.A. Rawool, K.K. Yadav, V. Polshettiwar, Defective TiO_2 for photocatalytic CO_2 conversion to fuels and chemicals, Chem. Sci. 12 (2021) 4267–4299.

[59] Y. Ji, Y. Luo, New mechanism for photocatalytic reduction of CO_2 on the anatase TiO_2(101) surface: the essential role of oxygen vacancy, J. Am. Chem. Soc 138 (2016) 15896–15902.

[60] H. Gao, J. Zhang, F. Zhang, J. Jing, W.-Y. Li, Enhanced formic acid production for CO_2 photocatalytic reduction over Pd/H-TiO_2 catalyst, Front. Chem. Sci. Eng. 18 (2024) 134.